Eur Biophys J (2011) 40:165–174
DOI 10.1007/s00249-010-0636-5

ORIGINAL PAPER

Time-resolved release of calcium from an epithelial cell monolayer during mucin secretion

Sumitha Nair · Rohit Kashyap · Christian Laboisse · Ulrich Hopfer · Miklós Gratzl

Received: 26 May 2010 / Accepted: 6 October 2010 / Published online: 26 October 2010

Abstract A significant amount of Ca^{2+} is contained in secretory mucin granules. Exchange of Ca^{2+} for monovalent cations drives the process of mucin decondensation and hydration after fusion of granules with the plasma membrane. Here we report direct observation of calcium secretion with a Ca^{2+} ion-selective electrode (ISE) in response to apical stimulation with ATP from HT29-Cl.16E cells, a subclone of the human colonic cancer cell line HT29. No increase in Ca^{2+} level was seen for the sister cell line Cl.19A, which lacks mucin granules, or for Cl.16E cells after inhibition of granule fusion with wortmannin. Further, the measured concentration was used to estimate the time-resolved rate of release of Ca^{2+} from the cell monolayer, by use of a deconvolution-based method developed previously (Nair and Gratzl in Anal Chem 77:2875–2881, 2005). The results argue that Ca^{2+} release by Cl.16E cells is associated specifically with mucin secretion, i.e., that the measured Ca^{2+} increase in the apical solution is derived from granules after fusion and mucin exocytosis. The Ca^{2+} ISE in conjunction with deconvolution provides a minimally disturbing method for assessment of Ca^{2+} secretion rates. The release rates provide estimates of exocytosis rates and, when combined with earlier capacitance measurements, estimates of post-stimulation endocytosis rates also.

Keywords HT29-Cl.16E · Ion selective electrode · Exocytosis · Endocytosis · Voltage clamp · Capacitance

Introduction

Mucus is an exocrine secretion that lubricates and protects underlying epithelial cells of the various mucous membranes of the body (Verdugo et al. 1987; Moniaux et al. 2001). Mucus secretions consist mainly of water, electrolytes, and carbohydrate-rich gel-forming mucin glycoproteins (Verdugo 1990). Overproduction of mucus is characteristic of many respiratory diseases including asthma, chronic obstructive pulmonary disease, and cystic fibrosis (Rogers and Barnes 2006).

Mucins are stored in the apical portion of epithelial cells inside mucin granules in a highly condensed matrix. On the basis of video-enhanced microscopy it was thought that secretory proteins are entrapped inside the granules in a completely condensed and dehydrated core that was surrounded by a fluid aqueous phase (Verdugo 1990). Recent studies indicate that the mucin matrix inside the granule is not completely condensed, but rather comprises a mucin meshwork in a fluid phase in which the proteins and ions can slowly diffuse through pores and interact with matrix components (Perez-Vilar 2007). There is evidence that specific protein-mediated interactions are also important for intragranular organization of mucins in a condensed

Electronic supplementary material The online version of this article (doi:10.1007/s00249-010-0636-5) contains supplementary material, which is available to authorized users.

S. Nair · R. Kashyap · M. Gratzl (✉)
Department of Biomedical Engineering, Case School of Engineering, Case Western Reserve University, Cleveland, OH 44106, USA
e-mail: miklos.gratzl@case.edu

C. Laboisse
Institut National de la Santé et de la Recherche Médicale 94-04, Université de Nantes, 44035 Nantes, France

U. Hopfer
Department of Physiology and Biophysics, School of Medicine, Case Western Reserve University, Cleveland, OH 44106, USA

matrix (Perez-Vilar et al. 2006). Storage of mucin in a condensed state requires low pH and high concentrations of divalent or polyvalent cations to shield the negative charges of the polyanionic mucin chains (Verdugo 1990; Perez-Vilar 2007).

Ca^{2+} seems to be of major importance in charge shielding, as indicated by significant amounts of calcium found in secretory granules (Verdugo et al. 1987; Perez-Vilar 2007; Perez-Vilar et al. 2006; Paz et al. 2003). It has been proposed that loss of Ca^{2+} after granule fusion drives expansion of mucins into a polymer gel (Verdugo et al. 1987; Paz et al. 2003; Kuver et al. 2000). Granule fusion is initiated by formation of a secretory pore that enlarges with time. This would enable exchange of intragranular Ca^{2+} for monovalent cations from the extracellular space. This process increases the Donnan potential of the polymer matrix and thus would drive phase transition of mucins from a condensed network into a hydrated, highly expanded gel (Verdugo 1991). There is also evidence suggesting exchange of Ca^{2+} with K^+ during granule exocytosis (Marszalek et al. 1997; Nguyen et al. 1998), triggering a phase transition of the matrix.

Ca^{2+} release from isolated granules and individual goblet cells has been observed in real time by use of optical techniques (Nguyen et al. 1998; Quesada et al. 2001). Here we report direct observation of calcium secretion from HT29-Cl.16E cells, a subclone of the human colonic cancer cell line HT29 that is known to secrete mucins in response to apical purinergic stimulation (Merlin et al. 1994). A Ca^{2+} ion-selective electrode (ISE) placed close to Cl.16E monolayers indicated a significant increase in Ca^{2+} concentration on stimulation with ATP. There was no observable change in concentration when granule fusion was inhibited by pretreatment of cells with wortmannin, which prevents fusion by inhibition of phosphoinositide 3-kinases. Similarly, ATP addition did not elicit an increase in Ca^{2+} concentration at HT29-Cl.19A cells that contain no mucin granules. These results indicate that the Ca^{2+} increase at the Cl.16E cells was associated specifically with mucin secretion and the detected Ca^{2+} came from granules after fusion and exocytosis. Further, using the measured concentration we obtained the time-resolved release rate of Ca^{2+} from Cl.16A monolayers by use of a deconvolution method developed by two of the authors (Nair and Gratzl 2005). The Ca^{2+} release was found to be sustained over a ten-minute period, in contrast with the previously observed biphasic dynamics of Isc and Cl^- secretion by HT29-Cl.16E cells over the same duration (Nair et al. 2008). In this work we also demonstrate how the measured Ca^{2+} release from the mucin granules can be analyzed, together with earlier capacitance measurements (Bertrand et al. 1999), to estimate the rate of endocytosis post simulation.

Materials and methods

Materials

Dulbecco's modified Eagle's medium (DMEM), Ham's F12, and fetal bovine serum (FBS) were bought from Gibco (Grand Island, NY, USA). Vitrogen is a product of Celtrix Lab (Palo Alto, CA, USA). All chemicals for the Ca^{2+} ion-selective electrode were purchased from Fluka (Ronkonkoma, NY, USA). ATP, Phorbol-12-myristate-13-acetate (PMA) and other chemicals were bought from Sigma Chemical (St Louis, MO, USA).

Cell culture

HT29-Cl.16E and HT29-Cl.19A cells were propagated in Falcon culture flasks (25 cm^2) in a humidified atmosphere of 95% air and 5% CO_2 at 37°C. The cells were fed every day with DMEM supplemented with 10% heat-inactivated FBS and 4 mM L-glutamine. The passage numbers for the reported experiments were between 30–47 and 27–35 for HT29-Cl.16E and HT29-Cl.19A cells, respectively.

The cells were grown on Millicell-CM porous culture inserts (area: 0.6 cm^2) coated with Vitrogen®. Cl.16E cells were seeded at a density of 1.2×10^6 per filter and Cl.19A at a density of 0.5×10^6 per filter. The cells became visually confluent after one week and were used for secretion studies 12–18 days after seeding. The cell monolayers had resistances of 530 ± 30 ($n = 12$) and 440 ± 30 ($n = 4$) $\Omega\ cm^2$ for Cl.16E and Cl.19A cells, respectively.

Apparatus

Electrophysiology

An Ussing-type chamber (Analytical Bioinstrumentation, Cleveland, OH, USA) constructed to accept Millicell-CM inserts was used for transepithelial electrophysiology measurements. The chamber was modified to accept four electrodes for the voltage clamp (model 558-C-5; Bioengineering Department, University of Iowa, Iowa City, IA, USA) (two apical and two basal electrodes) and an ion-selective electrode (ISE) and reference electrode in the apical compartment as shown in Fig. 1. Figure 1. is not drawn to scale; the current electrodes were placed as far from the monolayer as possible to achieve uniform current density. The current electrode is a platinum wire 5–10 mm in length that was bent to form a coil-like arrangement to achieve larger surface area than the voltage electrodes. An electrode placed close to the cell monolayer will disturb the electric field generated by the current flow emanating from the cells. This will generate a voltage drop in the medium directly under the ISE parallel to the monolayer

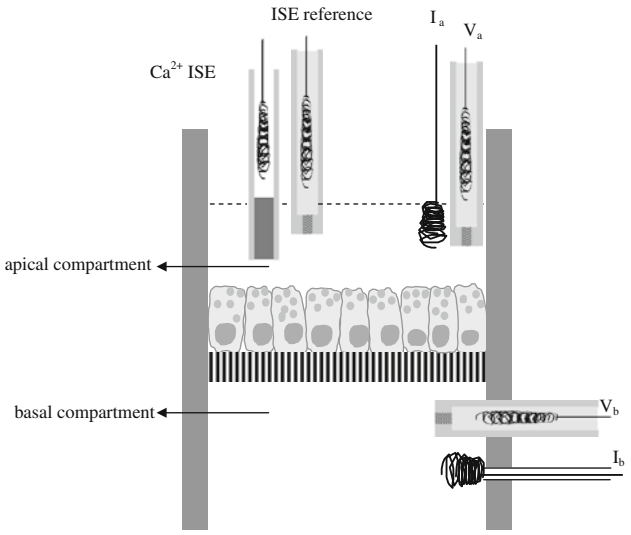

Fig. 1 Experimental arrangement to monitor Ca^{2+} release that accompanies mucin exocytosis in a confluent monolayer of HT29.Cl.16E cells. A standard four-electrode setup is used for voltage clamp: I_a and I_b are current passing platinum electrodes, and V_a and V_b are Ag/AgCl electrodes with liquid junctions on the apical and basolateral sides. The apical side of the Ussing chamber comprised two additional electrodes: a Ca^{2+} ISE and a ISE reference

and was estimated to be ~0.2 mV as discussed in Online Resource 1.

The chamber was grounded through the voltage clamp setup, which used an apical reference electrode independent of the ISE reference. Fluid resistance was compensated for, by using a blank Millicell-CM insert. The potential of the Ca^{2+} ISE during measurements was recorded with a high-input-impedance differential amplifier (PHM 84, Radiometer, Cleveland, OH, USA). The current output from the clamp and the voltage of the ISE were digitized and stored in a computer. During the experiment all solutions and the chamber were maintained at 37°C in a plexiglass incubator.

Reference electrodes and Ca^{2+} ion-selective electrode

The reference electrodes for the voltage clamp and for the Ca^{2+} ISE were each made of 18-gauge shrink Teflon tubing (Small Parts, Miami Lakes, FL, USA). One end of the tubing was sealed with a ceramic plug. The electrode body was back-filled with internal filling. A Ag|AgCl ($d \sim 1$ mm) wire was inserted into the electrode and parafilm was used to seal the electrode body and the wire together. Further details of the fabrication of the reference electrode can be found elsewhere (Nair et al. 2008).

Secretion of Ca^{2+} ions was monitored with a Ca^{2+} ISE. The electrode body was made from hard poly(vinyl chloride) (PVC) tubing (o.d. ~1.5 mm); the Ca^{2+}-selective liquid membrane was constructed from a cocktail of (by wt): 1% Ca^{2+} ionophore ETH 129, 65% 2-nitrophenyl octyl ether, 33% high-molecular-weight PVC, and 1% K^+ tetrakis(4-chlorophenyl)borate, dissolved in tetrahydrofuran. The membrane was deposited by dipping one end of the PVC tubing into the cocktail. If the membrane was not contiguous after 10 min of drying time the dipping step was repeated. The electrode was then allowed to dry for 4–6 h before further processing. The electrode body was filled with 0.1 M $CaCl_2$ and an Ag|AgCl internal reference electrode was inserted. Finally, the fully assembled Ca^{2+} ISE was conditioned overnight and calibrated in low-Cl^- and low-Ca^{2+} Ringer solution before and after each experiment. The data were least squares fit with the Nernst equation. Sensitivity was verified in situ by addition of known Ca^{2+} concentrations to the apical compartment. Electrode response was log–linear from 10^{-5} to 10^{-1} M with a close to theoretical (30.8 mV/decade) sensitivity ranging between 29.5 and 30.7 mV/decade at 37°C. Response time (90% of total change in potential) of the ISE was less than 20 s. The electrodes were stable over a period of 2 h with a mean potential drift of less than 1 mV/h.

Experimental procedures

Short-circuit current (Isc) and Ca^{2+} ISE measurements

A monolayer of Cl.16E or Cl.19A cells on Millicell-CM filter was placed in the Ussing-type chamber. The basolateral compartment was perfused with normal Ringer solution whereas the apical compartment was perfused with low-Ca^{2+} (60 μM)–low-Cl^- (2.1 mM) Ringer solution. Normal Ringer solution contained: 114 mM NaCl, 4 mM KCl, 1.25 mM $CaCl_2$, 1 mM $MgCl_2$, 10 mM HEPES, and 25 mM D-glucose. The low-Ca^{2+}-low-Cl^- solution contained: 114 mM Na gluconate, 4 mM K gluconate, 60 μM $CaCl_2$, 1 mM $MgCl_2$, 10 mM HEPES, and 25 mM D-glucose. The pH of the solutions was adjusted to 7.3 ± 0.1 with NaOH. The Ca^{2+} ion-selective electrode was positioned ~50 μm above the monolayer with a micromanipulator under visual control by first gently touching the monolayer with the electrode and then retracting it. Before each experiment, the voltage output of the clamp was adjusted to zero to compensate for any asymmetry in the voltage-sensing electrodes. The transepithelial potential was clamped to zero and the short-circuit current (Isc) measured. Perfusion of the apical chamber was stopped for a bolus of 1 mM ATP + 50 nM PMA added to initiate secretion and during subsequent measurements. Data were collected shortly before addition of the secretagogue and for 9–10 min after addition. The inclusion of 50 nM PMA in the ATP solution increased the Isc response in the monolayers used in this

study, presumably by partially activating protein kinase C and thereby increasing the sensitivity of secretion to purinergic stimulation; 50 nM PMA by itself had no effect on the Isc.

The experiments described in this work were conducted under conditions of low Cl^- in the apical solution and in the presence of PMA, so the conditions for Isc measurement in these studies are the same as those in previous work (Nair et al. 2008). This allows us to verify that electrolyte secretion in these experiments is comparable to that in previous studies (Nair et al. 2008) and that the increase in calcium concentration in the apical compartment is not linked to some mechanistic changes in the electrolyte secretion pathways. The identical experimental conditions also enable us to compare the dynamics of Isc measured in the previous work and that obtained in this work with the dynamics of Ca^{2+} release that is measured.

The low apical Cl^- solution increases the Cl^- current (Isc) and is commonly used in similar secretory experiments with bronchial cells for the same purpose (Liu et al. 2007). In addition a robust Isc signal was desirable in these experiments for timing of cell stimulation by agonists.

Estimation of a hypothetical basal-to-apical Ca^{2+} flux

Asymmetric Ca^{2+} on the two sides of the monolayer could theoretically produce a diffusional basal-to-apical flux of Ca^{2+}. The maximum possible diffusional flux of Ca^{2+} through the paracellular pathway because of this asymmetry was modeled as established previously (Nair et al. 2008). The predicted theoretical ISE response to such hypothetical flux was compared with the measured ISE potentials. The measured changes were far greater and different in dynamics both during the baseline and stimulated period, suggesting that, even in the worst case, hypothetical paracellular net movement of Ca^{2+} cannot explain the Ca^{2+} flux measured during stimulation.

Back-calculation of secretion flux from measured concentration data

Diffusion of the released Ca^{2+} from the luminal surface of the monolayer is essentially planar in nature (Nair and Gratzl 2005). The measured concentration can thus be expressed as a convolution of release rate (secretory flux) at the cells with the impulse response function of planar diffusion at the height of the ISE above the monolayer (Nair and Gratzl 2005). Secretion flux of Ca^{2+} is therefore obtained by deconvolution of mass transport from the measured concentration. This operation was performed using a novel deconvolution algorithm based on function shape optimization (Nair and Gratzl 2005). Important experimental conditions for the deconvolution are the diffusion constant for Ca^{2+} (0.79×10^{-5} cm^2 s^{-1}; from Part and Lock 1983) and the distance of the ISE from the cell monolayer ($\sim$50 μm). This distance of $\sim$50 μm is 5–7 times of the cellular diameter and is chosen to average the signal from several cells while retaining sufficient signal and time resolution to extract useful information.

Results

The HT29-Cl.16E cell line secretes mucins and electrolytes when stimulated by luminal ATP (Merlin et al. 1994, 1996; Bertrand et al. 1999) and thus provides a model for identifying biological processes associated specifically with mucin release from epithelia. The sister cell line HT29-Cl.19A secretes electrolytes in response to stimulation but lacks secretory granules (Merlin et al. 1996) and hence serves as a control. The experimental arrangement used to measure Ca^{2+} efflux during mucin secretion comprised a Ca^{2+} ISE and a reference electrode in the apical compartment in addition to the voltage and current electrodes used for short circuit current (Isc) measurements, as shown in Fig. 1. The ISE is placed at a distance of $\sim$50 μm from the cell monolayer with its reference electrode remotely positioned. In the experiments reported here significant secretion of Ca^{2+} from mucin granules of Cl.16E cells was observed. The level and time course of Ca^{2+} secretion provided time-resolved information on the degranulation process and its dynamics.

Purinergic stimulation of a monolayer of Cl.16E cells that contain mucin granules

Addition of 1 mM ATP + 50 nM phorbol-12-myristate-13-acetate (PMA) to the apical compartment of the Ussing chamber led to an immediate increase in Isc (Fig. 2a, solid line). After a lag of $\sim$1 min the Ca^{2+} ISE potential also began to increase (not shown), indicating an increase in Ca^{2+} concentration (Fig. 2b, solid line) $\sim$50 μm from the cells. The average maximum potential change in response to stimulation was 8.5 ± 3.5 mV ($n = 8$).

This implies an increase in Ca^{2+} concentration of 53.5 ± 14.6 μM above the baseline level of 60 μM. The Ca^{2+} flux density *at the cell monolayer*, indicated as a solid line in Fig. 2c, was computed by deconvolution of diffusional mass transport from the measured concentration, as briefly explained in the section "Back-calculation of secretion flux from measured concentration data". Further details of the deconvolution method can be found elsewhere (Nair and Gratzl 2005). The data for Cl.16E cells shown in Fig. 2 are from an experiment that is representative of experiments on eight separate filters.

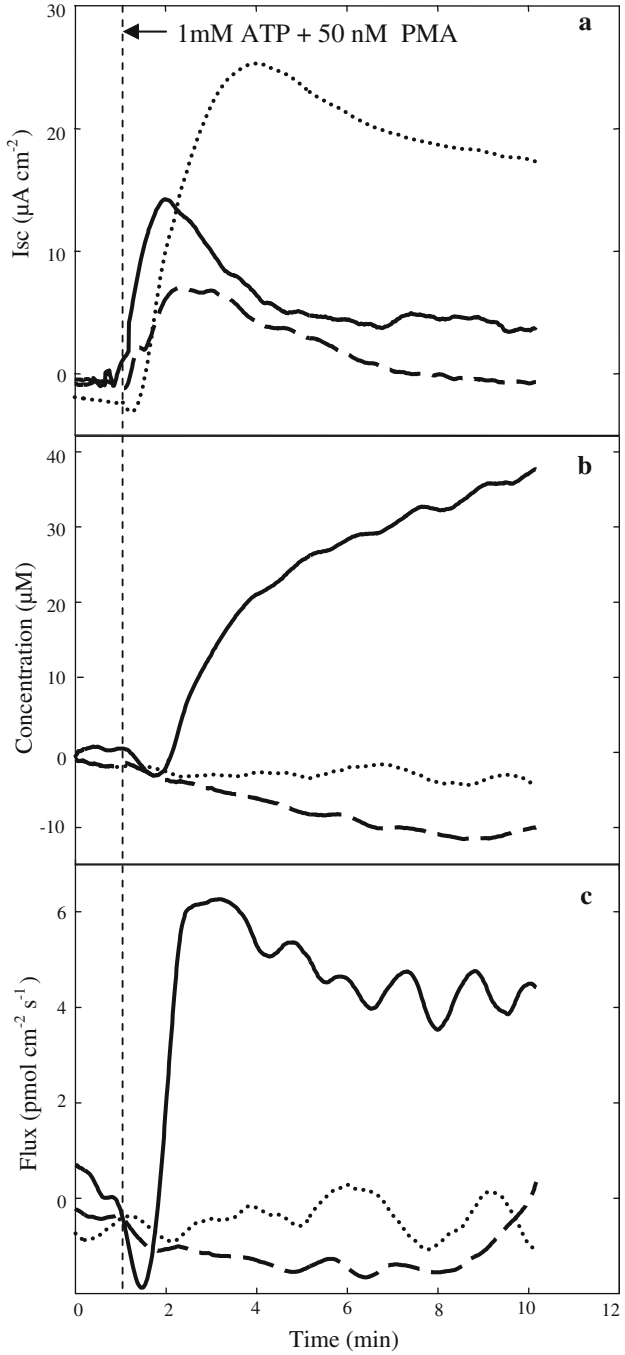

Fig. 2 Ca^{2+} secretion from mucin granules in a monolayer of HT29Cl.16E cells stimulated apically with 1 mM ATP + 50 nM PMA. Real time Isc and Ca^{2+} concentrations recorded by the ISE in response to purinergic stimulation on the apical side is shown in *Panels a* and *b*, respectively. The Ca^{2+} fluxes back-calculated from the measured concentration are shown in *Panel c*. *Solid lines*: HT29Cl.16E cells. *Dashed lines*: HT29Cl.16E cells pretreated with 100 nM wortmannin by incubation for 15 min. *Dotted lines*: HT29Cl.19A cells. Lack of ATP-mediated increase in Ca^{2+} flux from HT29Cl.19A cells (*Panel c*: *dotted line*) and Cl.16E cells pretreated with Wortmannin (*Panel c*: *dashed line*) indicates that the Ca^{2+} efflux from Cl.16 E cells (*Panel c*: *solid line*) in response to ATP stimulation is associated with mucin secretion

To establish that mucin granules were indeed the source of the measured increase in Ca^{2+} concentration, two different control experiments were conducted.

1. Similar measurements were done with the sister cell line HT29-Cl.19A. These cells do not have mucin granules but respond to apical stimulation by external ATP with electrolyte secretion (Merlin et al. 1996).
2. Before purinergic stimulation, Cl.16E cells were pre-incubated with 100 nM wortmannin to block fusion of mucin granules. This treatment has been shown to effectively block granule fusion in Cl.16E cells (Merlin et al. 1996).

Purinergic stimulation of Cl.19A cells that do not contain mucin granules

The Isc measurements on Cl.19A cells in response to apical stimulation with 1 mM ATP + 50 nM PMA are shown in Fig. 2a (dotted line). Consistent with previous observations (Merlin et al. 1996) the increase in Isc in response to purinergic stimulation of Cl.19A cells was ~70% higher than for Cl.16E cells. There was, however, no local increase in Ca^{2+} concentration (Fig. 2b, dotted line). This indicates that Ca^{2+} ions were not secreted in response to stimulation. Because Cl.19A and Cl.16E are similar except for the presence of mucin granules in Cl.16E cells this indicates that the mucin granules are the source for Ca^{2+} release observed in Cl.16E cells. The corresponding nominal Ca^{2+} flux density *at the cells* is shown as dotted line in Fig. 2c. The results for Cl.19A cells shown in Fig. 2 are from an experiment that is representative of experiments on three separate filters.

Purinergic stimulation of mucin-granule-containing Cl.16E cells pretreated with an inhibitor of granule fusion

Cl.16E cells were pretreated with 100 nM wortmannin for 15 min before stimulation with external ATP. The Isc response is inhibited by ~40% compared with untreated cells (Fig. 2a, dashed line). This observation is consistent with previous results (Merlin et al. 1996). The Ca^{2+} ISE indicated no increase in Ca^{2+} concentration with purinergic stimulation, as was the case with Cl.19A cells. The corresponding nominal Ca^{2+} efflux back-calculated from the measured concentrations is shown as dashed line in Fig. 2c. The data for wortmannin treated Cl.16E cells shown in Fig. 2 are from an experiment that is representative of experiments on three separate filters.

Discussion

Comparison of calcium secretion from Cl.16E cells, Cl.19A cells, and Cl.16E cells pretreated with wortmannin

The experiments with HT29 clones that differ in mucin secretory capacity and with inhibitors of mucin secretion in HT29 Cl.16E revealed large changes in the ratio of Ca^{2+} secretion to Isc, indicating that mucin granules are the source of a local increase in Ca^{2+} concentration when Cl.16E cells are stimulated with apical ATP. Thus the back-calculated Ca^{2+} flux contains information about exocytosis of mucin granules. Future work will be required to determine with greater precision the delay of Ca^{2+} secretion relative to Isc and to determine the causes. Causes could be technical (e.g., response time of electrode) or biological (e.g., delay of granule fusion and release of Ca^{2+} secretion to Cl^- secretion across the plasma membrane).

Comparison of calcium secretion from Cl.16E cells with Isc and previously measured chloride secretion from the same cell line

It is noteworthy that the dynamics of Ca^{2+} secretion is different from the dynamics of Cl^- secretion measured in previous studies (Nair et al. 2008). The Cl^- secretion more closely follows the dynamics of the simultaneously measured Isc. This close coupling is expected as Cl^- movement through apical channels is associated with a transepithelial current. Conversely a lag in Ca^{2+} secretion is consistent with granule fusion and release of intragranular Ca^{2+} which would not contribute to a transepithelial current. Furthermore, only a part of cellular Cl^- secretion, namely the wortmannin-sensitive portion ($\sim$40% of Isc) is associated with granule fusion and mucin exocytosis (Merlin et al. 1996). Activation of Cl^- channels in the constitutive plasma membrane would be expected to immediately contribute to Isc whereas contributions from activated Cl^- channels in the granule membrane would have to wait for granule fusion to functionally become part of the plasma membrane.

Effect of variability in diffusion constant and electrode placement on the estimated flux

A diffusion constant of 0.79×10^{-5} cm^2 s^{-1} for Ca^{2+} (Part and Lock 1983) was used in the optimization to obtain flux information from the measured concentration. The effect of $\pm$20% uncertainty in the diffusion constant on the flux estimates was evaluated; the results are summarized in Table 1. The peak of estimated Ca^{2+} flux shows $\sim$4% variation for a 10% relative variability in diffusion constant.

Table 1 Effect of variability in diffusion constant on Ca^{2+} flux density back-calculated with shape optimization

Diffusion constant (cm^2 s^{-1})	Peak of back-calculated Cl^- flux density (pmol cm^{-2} s^{-1})
0.95×10^{-5} (0.79×10^{-5} + 20%)	6.78
0.79×10^{-5} (diffusion constant in mucus)	6.27
0.63×10^{-5} (0.79×10^{-5} − 20%)	5.70

The electrode distance from the monolayer was assumed to be 50 μm

Table 2 Effect of variability in distance on Ca^{2+} flux density back-calculated with shape optimization

Distance (μm)	Peak of back-calculated Ca^{2+} flux density (pmol cm^2 s^{-1})
45	6.18
50	6.27
55	6.29

The Ca^{2+} diffusion constant was assumed to be 0.79×10^{-5} cm^2 s^{-1}

In addition to the diffusion constant the deconvolution algorithm also uses the electrode distance from the monolayer as a variable. An electrode distance of 50 μm was used in the optimization. Table 2 summarizes the effects of $\pm$5 μm variability in electrode placement on the back-calculated flux. The peak of Ca^{2+} flux shows $\sim$1% variation for 10% variability in electrode positioning.

Validation of the diffusion model used to reconstruct secretion flux of Ca^{2+} from measured concentration

Mucin release from fused granules and its expansion is triggered by exchange of Ca^{2+} ions for monovalent cations (Verdugo et al. 1987; Verdugo 1990; Perez-Vilar 2007; Perez-Vilar et al. 2006). Thus, exocytosis at the cells, ion exchange in the expanding mucus, and diffusion away from the cells are the processes that determine the concentration of Ca^{2+} measured by the electrode. The deconvolution approach that we use to reconstruct the rate of Ca^{2+} secretion assumes that ion exchange is faster than either exocytosis or diffusion and thus has negligible effect on the measured concentration. This assumption is validated as follows.

The total amount of Ca^{2+} that has moved to the apical compartment from the Cl.16E monolayer was assessed by mixing the apical chamber at the end of the recording and measuring the resulting concentration (Nair et al. 2008). Multiplying the obtained concentration minus the baseline value of 60 μM by the initial volume (0.3 mL) of the apical

medium and neglecting possible fluid secretion, the net change in Ca^{2+} content during the entire experiment could be estimated. The total amount of secreted Ca^{2+} thus obtained was $\sim 1.77 \pm 0.06$ nmol per filter (filter area = 0.6 cm^2) over the measurement time of 10 min ($n = 8$). This amount can also be estimated from the integral of the computed flux and was found to be ~ 1.86 nmol per filter for the 10 min duration of the experiment analyzed in Fig. 2. If ion exchange was slow enough to significantly affect the measured concentration, the total cumulative Ca^{2+} efflux computed from continuous ISE recording using a model based purely on diffusion would differ from physical measurement of the total final Ca^{2+} increase by much more than 5%. This confirms that it is diffusion of Ca^{2+} from the cells to the sensor and not ion exchange that is rate limiting once the granule contents are exocytosed. Hence back-calculated Ca^{2+} flux is directly related to the exocytosis rate.

The good agreement between the total cumulative Ca^{2+} efflux computed from continuous recording of Ca^{2+} concentrations and physical measurement of total Ca^{2+} released at the end of the experiment is indicative of the robustness of the approach and validates the diffusion constant and electrode distance from the monolayer used in the optimization.

Dynamics of calcium secretion compared with measured change in capacitance

Previously, the net increase in membrane surface area due to purinergically stimulated mucin exocytosis in Cl.16E cells was monitored by means of membrane capacitance measurements (Bertrand et al. 1999). The change in capacitance in response to stimulation with different levels of ATP was measured together with Isc and DC resistance. The dynamics and amplitude of Isc in response to 3 mM ATP are closest to those obtained in this work, so the capacitance change in response to this stimulation was therefore used for comparison with the Ca^{2+} flux. We note that there could be discrepancies because of possible variability in the cultures, and the difference in ATP concentration used for stimulation. We nevertheless feel that it is useful to analyze the back-calculated Ca^{2+} flux on the basis of the capacitance data to derive principles that could be used to obtain greater insight into the process of exocytosis.

The measured change in total capacitance in response to stimulation contains information about both the basolateral and apical capacitance, but only the latter is affected by exocytosis. The apical capacitance can be obtained from the measured total capacitance as described elsewhere (Bertrand et al. 1999). It increases upon stimulation and reaches a peak value after approximately 3 min. It then undergoes rapid decay to approximately half of the peak value by 10 min post stimulation. It takes ~ 30 min for the apical capacitance to return to its basal value.

The back-calculated secretion flux of Ca^{2+}, as determined in this work, also reaches a peak within approximately the same time frame as the apical capacitance does. Ca^{2+} flux then decreases to $\sim 70\%$ of its peak value ~ 10 min after stimulation. Thus, Ca^{2+} secretion is likely to be sustained significantly longer than the 10-min duration of the experiments reported here. Its decay, however, seems to be significantly slower than the rate of decay in apical capacitance. This implies that endocytosis is significant during secretion and therefore its effect must be taken into account when interpreting the findings.

The peak in apical capacitance indicates that endocytosis rate also increases in response to stimulation but it takes about 3 min for it to "catch up" with the rate of exocytosis, because at the peak the two rates must be equal. This is followed by a period when the rate of endocytosis is higher than the rate at which membrane is added by exocytosis. During this time both endocytosis and exocytosis rates continue to remain higher than the basal rates. It takes ~ 30 min for the membrane surface area to return to its basal value. Thirty minutes after stimulation the exocytosis and endocytosis rates are once again equal, possibly reaching basal levels.

Estimate of Ca^{2+} concentration in mucin granules of HT29.Cl.16E cells

Previously the peak in capacitance of the apical membrane 3 min after stimulation was estimated to correspond to fusion of a minimum number of 42 and a maximum of 172 granules (1 μm in diameter) per goblet cell for a goblet cell density of 800,000 cells cm^{-2} (Bertrand et al. 1999). The back-calculated Ca^{2+} flux added up to 3 min can be used as an estimate of the amount of Ca^{2+} that was released during this period from the granules as a result of exocytosis. This information can then be translated to Ca^{2+} concentration in a granule by use of Eq. (1):

$$[Ca^{2+}]_{granule} = {}^{1}/_{(S_{goblet} \times N_T \times V_{granule})} \int_0^T Flux_{Ca^{2+}} dt \quad (1)$$

where $t = 0$ corresponds to the point of stimulation, $T = 3$ min, S_{goblet} (800,000 cells cm^{-2}) is the goblet cell density, N_T (42 or 172) is total number of granule fusions in time T (3 min) after stimulation, $V_{granule}$ (0.52×10^{-12} cc; assuming spherical granules with diameter of 1 μm) is the volume of a granule, and $Flux_{Ca^{2+}}$ is the back-calculated Ca^{2+} secretion flux. The total amount of Ca^{2+} released ~ 3 min after stimulation is 0.7 nmol cm^{-2}.

On the basis of Eq. (1), a capacitance peak that results from fusion of 42 granules would correspond to an intragranular Ca^{2+} concentration of 40 mM. If the capacitance peak was the result of 172 granule fusions the intragranular Ca^{2+} concentration would be 10 mM.

The estimates of the number of granule fusions used in these calculations were based on the measured "net" increase in apical capacitance which does not account for concurrent endocytosis. Taking endocytosis into account the number of granule fusions could be much higher than the net capacitance increase would indicate. As represented in Eq. (1), this would also translate into lower intragranular Ca^{2+} concentrations.

How low the estimate of intragranular Ca^{2+} concentration can be will depend on the total number of granule fusions over the measurement time period and the availability of granules per cell. An intragranular Ca^{2+} concentration of 10 mM corresponds to 550 granule fusions over the 10 min measurement time as estimated from Eq. (1), for $T = 10$ min. The potential number of 1 μm diameter granules in a typical goblet cell 30 μm in height and 6–8 μm in diameter, where the granules occupy one-fourth to one-third of the cell, was calculated to range from 410 to 960 (these estimates are adapted from the work done by Davis et al. 1992). The dynamics of back-calculated flux and the earlier capacitance measurements both point towards significant granule fusion even 15–20 min after stimulation. All of these, taken together, indicate that Ca^{2+} concentration inside the granule could be 10 mM or lower when 60–80% or more of the available granule pool is exocytosed. The calcium concentration inside mucin granules is therefore estimated to range from 10 to 40 mM. This is in agreement with reported calcium concentrations inside zymogen granules (~15 mM; Raraty et al. 2000) and secretory granules (from 1 to 200 mM; Nicaise et al. 1992).

Equation (1) above uses goblet cell density and granule diameter as variables and hence any variations in their values will affect the concentration estimates as discussed below. Equation (1) can be thought of as a simple algebraic equation with an inverse relationship between goblet cell density and calcium concentration inside the granule. It can be easily derived that a 20% increase in goblet cell density will reduce the estimate of calcium concentration by 16.7%. The estimate for calcium concentration will, on the other hand, increase by 25% for a 20% decrease in goblet cell density.

We also note that estimates of calcium concentration inside the granule would differ significantly for even minor variations in cell size and granule diameter. For example, the possible number of 1.5 μm diameter granules for the same goblet cell dimensions as described above would range from 120 to 284. In this case the estimated Ca^{2+} concentration inside the granule will be closer to the upper limit of 40 mM.

Reconstruction of endocytosis from measured Ca^{2+} flux and capacitance change

The increase in apical capacitance over the baseline (ΔC_A) in response to stimulation, obtained from the measured total capacitance, indicates the net change in apical membrane surface area. This is the difference between capacitance because of addition of membrane surface by exocytosis (C_{exo}) and that corresponding to membrane surface removed by endocytosis (C_{endo}), as shown in Eq. (2).

$$\Delta C_A = C_{exo} - C_{endo} \tag{2}$$

In Eq. (2), $\Delta C_A = {}^{1}/_{\left(C_T^{-1} - C_B^{-1}\right)} - C_A^{baseline}$, where C_T and C_B are the total capacitance and basolateral capacitance, respectively, and $C_A^{baseline}$ is the baseline apical capacitance.

As explained above, the rate of exocytosis is what predominantly limits the rate of release of Ca^{2+}. Hence the back-calculated flux is directly proportional to the exocytosis rate. Equation (2) can therefore be re-written in terms of back-calculated flux as follows:

$$\begin{aligned}\Delta C_A(t) &= C_{exo}(t) - C_{endo}(t) \\ &= k \int_0^t \mathrm{Flux}_{Ca^{2+}} dt \Big/ \left([Ca^{2+}]_{granule} \times V_{granule} \right) \\ &\quad - C_{endo}(t)\end{aligned} \tag{3}$$

In Eq. (3), k is the capacitance corresponding to the fusion of a single granule, which was estimated to be 31fF (Bertrand et al. 1999), and $\mathrm{Flux}_{Ca^{2+}}$ is the back-calculated Ca^{2+} secretion flux. Hence a median intragranular Ca^{2+} concentration of 25 mM was used in Eq. (4):

$$\begin{aligned}C_{endo}(t) &= k \int_0^t \mathrm{Flux}_{Ca^{2+}} dt \Big/ \left([Ca^{2+}]_{granule} \times V_{granule} \right) \\ &\quad - \Delta C_A(t)\end{aligned} \tag{4}$$

to reconstruct C_{endo} from back-calculated flux for a median basolateral capacitance of 15 μF cm^{-2}. Median basolateral capacitance was determined from previously reported (Bertrand et al. 1999) minimum and maximum estimates of 5 and 25 μF cm^{-2}. The corresponding exocytosis, endocytosis, and change in apical capacitance are shown in Fig. 3. In Eqs. (3) and (4) t represents time and is a running variable with a limit of 0–10 min (the entire measurement period).

The results shown in Fig. 3 indicate that the measured transient in total capacitance post stimulation is not indicative of the amount or time course of exocytosis. Significant endocytosis follows the onset of exocytosis, and

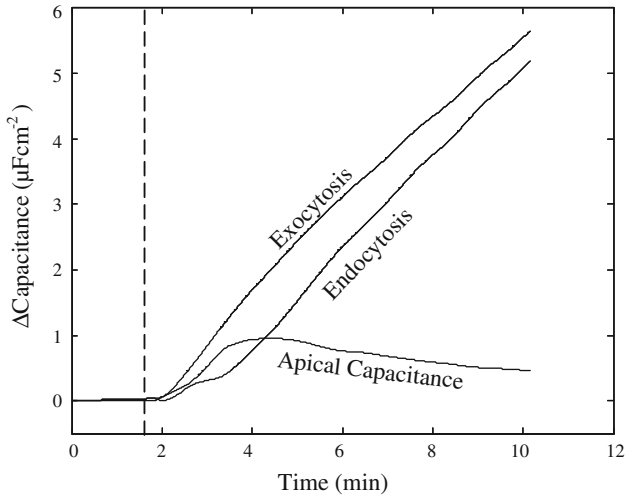

Fig. 3 Change in apical capacitance together with capacitance change that corresponds to exocytosis and endocytosis in response to apical purinergic stimulation. The change in apical capacitance was estimated from previously measured capacitance change in response to stimulation (Bertrand et al. 1999). Back-calculated flux was translated to capacitance added because of exocytosis, as shown in Eq. (3). The earlier (Bertrand et al. 1999) capacitance measurements were sparsely sampled with the shortest and longest time intervals between measurements being 30 and 60 s, respectively. The ISE measurements on the other hand were evenly sampled at 1-s intervals throughout the 10 min measurement period. (Note: The 1 s sampling rate that is used is much higher than that warranted by the 20 s response time of the electrode alone. The higher response time is justified by the fact that in order to estimate fluxes from the measured concentration a deconvolution operation needs to be performed. We have shown (Nair and Gratzl 2008) that to correctly reconstruct fluxes from measured concentrations the Nyquist criterion for the impulse response of diffusion must also be satisfied. The 1 s sampling rate that is used is just sufficient to satisfy the Nyquist criterion for the impulse response of diffusion.) Hence the apical capacitance data obtained from the measured total capacitance had to be interpolated every 1 s and smoothed using the Savitsky and Golay (1964) procedure before use in Eq. (4), to estimate the capacitance removed because of endocytosis. Interpolation and smoothing was done using "interp1" and "sgolay" functions, respectively, available in Matlab 7.0.4, Release 14 (The Mathworks, Natick, MA, USA). A second-order filter with a window length of seventy-five data points was used for smoothing

degranulation and retrieval of the granule membrane continue at a rate that slowly decreases over a long time during which apical capacitance decays significantly.

The basal endocytosis for the results shown in Fig. 3 is $\sim$0.012 pFcell^{-1}; endocytosis corresponding to the peak of the apical capacitance is 0.9 pFcell^{-1}. Basal endocytosis and that corresponding to ATP stimulation in HT29.Cl.16E cells are reported to range from 0.02–0.06 to 0.08–0.33 pFcell^{-1}, respectively. The results for endocytosis reported by Bertrand et al. (2006) are not expressed as a function of time and, therefore, cannot be directly compared with the results presented in this work. It is however noteworthy that the order of magnitude of endocytosis data reported by Bertrand et al. are comparable with those estimated in this work, despite the different methods used.

Conclusions

The experimental approach using an ion-selective electrode for measuring Ca^{2+} at the cells together with the capability of translating the measured concentration into flux have made it possible in this work to obtain the dynamics of Ca^{2+} release from mucin granules from an intact epithelial cell monolayer in a physiologically relevant Ussing chamber arrangement. The release rate of Ca^{2+} can be used to estimate the rate of degranulation. Independent information on degranulation is contained in the time course of measured total capacitance. This work demonstrates how the back-calculated flux together with capacitance data can be used to obtain information about intragranular calcium content, and endocytosis in response to stimulation.

The results presented in this work are the first quantitative real time-data on Ca^{2+} release from mucin granules in a confluent epithelial cell monolayer. The method for reconstructing the rates of concurrent exocytosis and endocytosis using release rate and capacitance as two pieces of independent information is also presented here for the first time, and can find applications in other contexts of cell physiology.

Acknowledgments The authors thank Mabintou Traore for performing early feasibility studies. This work was supported by funds from the National Institute of Health (Grant CA-61860 to MG), the Cystic Fibrosis Foundation (grants HOPFER99PO to UH and G813 to MG), and the Ohio Board of Regents Innovation Incentive Fellowship award to SN.

References

Bertrand CA, Laboisse CL, Hopfer U (1999) Purinergic and cholinergic agonists induce exocytosis from the same granule pool in HT29-Cl.16E monolayers. Am J Physiol 276:C907–C914

Bertrand CA, Laboisse C, Hopfer U, Bridges RJ, Frizzell RA (2006) Methods for detecting internalized, FM 1–43 stained particles in epithelial cells and monolayers. Biophys J 91:3872–3883. doi: 10.1529/biophysj.106.086983

Davis CW, Dowell ML, Lethem M, Van Scott M (1992) Goblet cell degranulation in isolated canine tracheal epithelium: response to exogenous ATP, ADP, and adenosine. Am J Physiol 262:C1313–C1323

Kuver R, Klinkspoor JH, Osborne WRA, Lee SP (2000) Mucous granule exocytosis and CFTR expression in gallbladder epithelium. Glycobiology 10:149–157

Liu X, Luo M, Zhang L, Ding W, Yan Z, Engelhardt JF (2007) Bioelectric properties of chloride channels in human, pig, ferret, and mouse airway epithelia. Am J Respir Cell Mol Biol 36(3):313–323. doi:10.1165/rcmb.2006-0286OC

Marszalek PE, Farrell B, Verdugo P, Fernandez JM (1997) Kinetics of release of serotonin from isolated secretory granules. II. Ion exchange determines the diffusivity of serotonin. Biophys J 73:1169–1183

Merlin D, Augeron C, Tien XY, Guo X, Laboisse CL, Hopfer U (1994) ATP- stimulated electrolyte and mucin secretion in the human intestinal goblet cell line HT29-Cl.16E. J Membr Biol 137:137–149

Merlin D, Guo X, Martin K, Laboisse CL, Landis D, Dubyak G, Hopfer U (1996) Recruitment of purinergically stimulated Cl^- channels from granule membrane to plasma membrane. Am J Physiol 271:C612–C619

Moniaux N, Escande F, Porchet N, Aubert JP, Batra SK (2001) Structural organization and classification of the human mucin genes. Front Biosci 6:D1192–D1206

Nair S, Gratzl M (2005) Deconvolution of concentration recordings at live cell preparations via shape error optimization. Anal Chem 77:2875–2881. doi:10.1021/ac048229a

Nair SP, Gratzl M (2008) Effects of sampling rate on the interpretation of cellular transport measurements. Anal Chem 80:7684–7689. doi:10.1021/ac800842m

Nair S, Kashyap R, Laboisse CL, Hopfer U, Gratzl M (2008) Time resolved secretion of chloride from a monolayer of mucin-secreting epithelial cells. Eur Biophys J 37:411–419. doi:10.1007/s00249-007-0226-3

Nguyen T, Chin WC, Verdugo P (1998) Role of Ca^{2+}/K^+ ion exchange in intracellular storage and release of mucin. Nature 395:908–912. doi:10.1038/27686

Nicaise G, Maggio K, Thirion S, Horoyan M, Keicher E (1992) The calcium loading of secretory granules. A possible key event in stimulus-secretion coupling. Biol Cell 75(2):89–99

Part P, Lock RA (1983) Diffusion of calcium, cadmium and mercury in a mucous solution from rainbow trout. Comp Biochem Physiol C 76:259–263

Paz HB, Tisdale AS, Danjo Y, Spurr-Michaud SJ, Argüeso P, Gipson IK (2003) The role of calcium in mucin packaging within goblet cells. Exp Eye Res 77:69–75. doi:10.1016/S0014-4835(03)00084-8

Perez-Vilar J (2007) Mucin granule intraluminal organization. Am J Respir Cell Mol Biol 36:183–190. doi:10.1165/rcmb.2006-0291TR

Perez-Vilar J, Mabolo R, McVaugh CT, Bertozzi CR, Boucher RC (2006) Mucin granule intraluminal organization in living mucous/goblet cells roles of protein post-translational modifications and secretion. J Biol Chem 281:4844–4855. doi:10.1074/jbc.M510520200

Quesada I, Chin WC, Steed J, Campos-Bedolla P, Verdugo P (2001) Mouse mast cell secretory granules can function as intracellular ionic oscillators. Biophys J 80:2133–2139

Raraty M, Ward J, Erdemli G, Vaillant C, Neoptolemos JP, Sutton R, Petersen OH (2000) Calcium-dependent enzyme activation and vacuole formation in the apical granular region of pancreatic acinar cells. PNAS 97(24):13126–13131

Rogers DF, Barnes PJ (2006) Treatment of airway mucus hypersecretion. Ann Med 38:116–125. doi:10.1080/07853890600585795

Savitsky A, Golay MJE (1964) Smoothing and differentiation of data by simplified least squares procedures. Anal Chem 36:1627–1639. doi:10.1021/ac60214a047

Verdugo P (1990) Goblet cell secretion and mucogenesis. Ann Rev Physiol 52:157–176. doi:10.1146/annurev.ph.52.030190.001105

Verdugo P (1991) Mucin exocytosis. Am Rev Respir Dis 144:S33–S37

Verdugo P, Deyrup-Olsen I, Aitken M, Villalon M, Johnson D (1987) Molecular mechanism of mucin secretion: I. The role of intragranular charge shielding. J Dent Res 66:506–508. doi:10.1177/00220345870660022001